REVIEWS

Journal of Semiconductors
(2020) 41, 091703
doi: 10.1088/1674-4926/41/9/091703

Regulation of surface properties of photocatalysis material TiO_2 by strain engineering

Jian Zheng and Dajun Shu†

National Laboratory of Solid State Microstructures and School of Physics, Nanjing University, Nanjing 210093, China

Abstract: As a promising photocatalysis material, TiO_2 has long been studied by experimental and theoretical methods. The external strain could affect the catalytic reactivity of TiO_2 significantly due to the difference in surface elastic properties of different surface structures with different surface adsorption or defects. This article reviews our recent work by using density function theory calculations on the effect of strain on the TiO_2 surface properties, including surface relative stability, surface defects, surface adsorption and dissociation.

Key words: semiconductor theory; material; thin film

Citation: J Zheng and D J Shu, Regulation of surface properties of photocatalysis material TiO_2 by strain engineering[J]. *J. Semicond.*, 2020, 41(9), 091703. http://doi.org/10.1088/1674-4926/41/9/091703

1. Introduction

Titanium dioxide is a promising photocatalysis material, which also has wide applications in heterogeneous catalysis, solar cells, gas sensor, etc[1–5]. The surface of TiO_2 has been extensively studied for many years due to its essential role in the applications. Especially, surface defects have been proved to be vital for surface reactivity. For instance, surface oxygen vacancies are reactive sites for water and other molecules[6]. It is desirable to use external field to control the surface properties in order to improve the surface reactivity of TiO_2.

Strain field is unavoidable in fabrication of nanostructures and thin film[7, 8]. It has been demonstrated that the band structure of TiO_2 can be changed by using strain[9]. Besides, the surface properties can also be engineered by strain. We have paid our attention on the strain effect on the surface of TiO_2 since 2008, and found that the strain can change many aspects of the surface properties, such as the surface energy, the distribution of surface defects, surface adsorption and dissociation[10–15].

In this paper, we review our work on the strain engineering of the surface properties of TiO_2. The following section is arranged as follows. In the second section, we will first introduce the simple theoretical background on the strain engineering. In the third section, we will discuss how the strain can be used to improve the relative percentage of the reactive surface. In the fourth and fifth sections, the thermodynamic and kinetic properties of oxygen vacancies under strain are reviewed, respectively. In the sixth and seventh sections, the effect of strain on the surface adsorption on stoichiometric and reduced TiO_2(110) are reviewed, respectively.

2. Elastic properties of TiO_2 surface

The structure and thus the properties of a bulk material respond to the external strain differently according to its bulk elastic properties. The bulk elastic properties of TiO_2 are described by six independent elastic constants. The bulk modulus and Young's modulus can be further calculated by these independent elastic constants. The results are presented in Table 1, including our own calculations based on the density functional theory (DFT)[13].

Similar to the case of a bulk material, the response of a surface to the external strain depends on the surface elastic properties. Generally speaking, different surface structures also have different surface elasticity. Therefore, the thermodynamic equilibrium surface structures would adjust themselves according to the external strain, and the surface properties change with the strain correspondingly.

The surface elastic properties can be described mainly by the surface stresses and surface elastic constants, which are defined as follows[19],

$$\sigma_{\alpha\beta} = \frac{1}{A_L}\frac{\partial(A_L\gamma_L)}{\partial\varepsilon_{\alpha\beta}} = \frac{\partial\gamma_L}{\partial\varepsilon_{\alpha\beta}},$$
$$S_{\alpha\beta\alpha'\beta'} = \frac{\partial\sigma_{\alpha\beta}}{\partial\varepsilon_{\alpha'\beta'}} = \frac{\partial^2\gamma_L}{\partial\varepsilon_{\alpha\beta}\partial\varepsilon_{\alpha'\beta'}}. \quad (1)$$

Here A_L and γ_L are the area of the surface and the Lagrangian surface energy per unit area in an unstrained state, respectively. The indices are 1 or 2, denoting the two orthogonal directions of a surface. To investigate the interplay between external strain and the surfaces, whether intrinsic or defective, we first of all calculated the surface energies of stoichiometric or defective surfaces with variation of external strain, from which the surface elasticity in different situations are derived according to Eq. (1). Then, the surface energy under arbitrary small strain can be calculated according to the continuum elastic theory. For instance, if the in-plane strains are ε_{11} and ε_{22}, the surface energy can be calculated as follows,

$$\gamma(\varepsilon) = \gamma(0) + \sigma_{11}\varepsilon_{11} + \sigma_{22}\varepsilon_{22} + \frac{1}{2}\varepsilon_{11}^2 S_{1111} + \frac{1}{2}\varepsilon_{22}^2 S_{2222} + \varepsilon_{11}\varepsilon_{22}S_{1122}. \quad (2)$$

Correspondence to: D J Shu, djshu@nju.edu.cn
Received 30 JUNE 2020; Revised 24 JULY 2020.

Table 1. The elastic constant C_{ij}, bulk modulus (B), Young's modulus along the a axis (Y_a), along the in-plane r direction (Y_r), and along the c axis (Y_c) of TiO_2 rutile and anatase phases, in units of GPa. This table is adapted from Ref. [13].

Parameter	C_{11}	C_{12}	C_{13}	C_{33}	C_{44}	C_{66}	B	Y_c	Y_r	Y_a
Rutile										
PW91[12]	265	179	151	472	116	211	209	369	348	138
Phonon[16]	269	189	166	506	105	217	219	386	349	130
PBE[17]	261	132	137	456	117	204	187	360	311	182
Exp[18]	268	175	147	484	124	190	212	386	354	147
Anatase										
PW91[12]	331	144	141	189	46	59	173	105	264	219
Phonon[16]	333	143	140	198	39	57	176	116	278	226
PBE[17]	311	150	138	191	51	59	172	108	262	199

Table 2. The calculated surface energy and surface mechanical properties of rutile and anatase phases. γ, σ, and S denote surface energy, surface stress, and surface elastic constant, respectively. Subscripts 11 and 22 denote the directions along [100] and [010] for (001) surface, [010] and [001] for (100) surface, $[10\bar{1}]$ and [010] for (101) surface, $[1\bar{1}0]$ and $[00\bar{1}]$ for (110) surface. The units are in J/m^2. This table is adapted from Ref. [13].

Parameter	γ	σ_{11}	σ_{22}	S_{1111}	S_{2222}	S_{1122}
Rutile						
(110)	0.44	2.52	1.14	−73.81	−17.67	−26.30
(100)	0.70	−1.74	1.28	−20.64	−2.88	−9.75
(101)	1.03	−0.08	0.16	−24.62	−25.38	−21.88
(001)	1.30	1.27	1.27	−8.27	−8.27	−15.80
Anatase						
(101)	0.52	0.77	2.06	41.33	−2.21	9.99
(100)	0.59	1.90	0.82	−1.31	4.40	−5.06
(001)	1.04	9.58	−2.13	2.64	2.64	−18.01
(110)	1.10	−2.09	1.31	−27.74	16.07	−2.17

Under a certain strain, by comparing the surface energies of different surface structures, one can expect to investigate the effect of strain on the surface thermodynamic or kinetic properties.

The surface elastic properties of TiO_2 are shown in Table 2, the calculation details of which can be found in Ref. [13]. The surface elastic constants S of rutile TiO_2 surface are always negative, whereas for anatase they are either positive or negative. Note that the significance of elastic constants of a surface are different from those in bulk. The elastic constants of a stable material must be positive, whereas negative surface elastic constants can occur, which means that the presentation of the surface makes TiO_2 in nanoscale softer than its bulk phase[13].

It is worthy to note that there is an odd–even oscillation of the surface properties of the relaxed TiO_2 in the thin film slab. For instance, for rutile (110) surface, although the surface energy and the band gap converge in a slab within about ten trilayers, the surface stresses in the $[1\bar{1}0]$ direction are still in obvious oscillation even when the thickness of the slab is 14 trilayers, as shown in Fig. 1. The thick-dependent surface stresses can be applied to change the relative stability of a thin film with different thickness, according to Eq. (2), by the strain along $[1\bar{1}0]$ direction. It suggests that one can selectively grow a thin film with a specific atomic layers by applying a suitable external strain.

3. Improving the percentage of reactive surfaces

Generally speaking, there is an intrinsic controversy between stability and reactivity in nature. The more reactive a surface is, the less stable it is, or the higher surface energy it is. According to the Wulff's theorem, it means that the percentage of a reactive surface is usually low. For example, in equilibrium anatase TiO_2, the most reactive (001) surface has a surface energy much larger than the (101) surface, as shown in Table 2. As a result, the area proportion of anatase (001) surface is no more than 3%, which strongly limits the reactive efficiency of TiO_2 in application as a photocatalyst[20–22].

Fortunately, the anatase (001) surface possesses the largest surface stress among all the surfaces, which is positive and occurs along the [100] direction. We therefore expect that the relative stability of (001) surface can be significantly improved by applying an compressive strain along the [100] direction, and thus its area percentage of anatase (001) according to Wulff construction. By first principle calculations, we have verified this[13]. As displayed in Fig. 2(a), under 5% biaxial compressive strain or compressive strain along [100], the area proportion of anatase (001) surface increases more than five times. In this way the external strain can be used to enhance the reactivity of TiO_2 catalyst.

4. Formation of surface oxygen vacancies under strain

Oxygen vacancies are the most common defects in transition metal oxide. The reduced materials usually show different physical properties compared to the stoichiometric one. In TiO_2, the oxygen vacancy (OV) has a low formation energy, and it has been experimentally found reactive in the surface reaction[23–30]. In order to investigate the influence of strain on the bulk and surface properties when different OVs are introduced, we first of all need to understand the responses of the formation of OVs to different external field[31, 32]. By using DFT calculations, we have found that external strain can modify the type of oxygen vacancy, which further influences the surface reactivity. Hereafter we refer the stoichiometric TiO_2 as s-TiO_2, while the TiO_2 with oxygen vacancies as r-TiO_2.

There are three types of oxygen atoms, bridging, in-plane and subbridging oxygen atoms, as shown in Fig. 3. Correspondingly, three different types of OV can be introduced by removing corresponding different types of oxygen atoms, namely BOV, IPOV and SBOV. We named different types of OVs to include the site of the defect. For example, 2-in-plane OV represents the OV formed by removing an in-plane oxygen atom in the second trilayer.

The OV formation energy can be calculated as follows,

$$E_{OV} = E_r - E_s + \frac{1}{2}E_{O_2}, \tag{3}$$

where E_{O_2} is the energy of the isolated O_2 molecular, and E_r and E_s stand for the energies of r-TiO_2 and s-TiO_2, respectively.

The OV formation energy as a function of OV depth is shown in Fig. 4(a). Obviously the 1-bridging OV is the most easily formed OV defect because of the lowest formation energy.

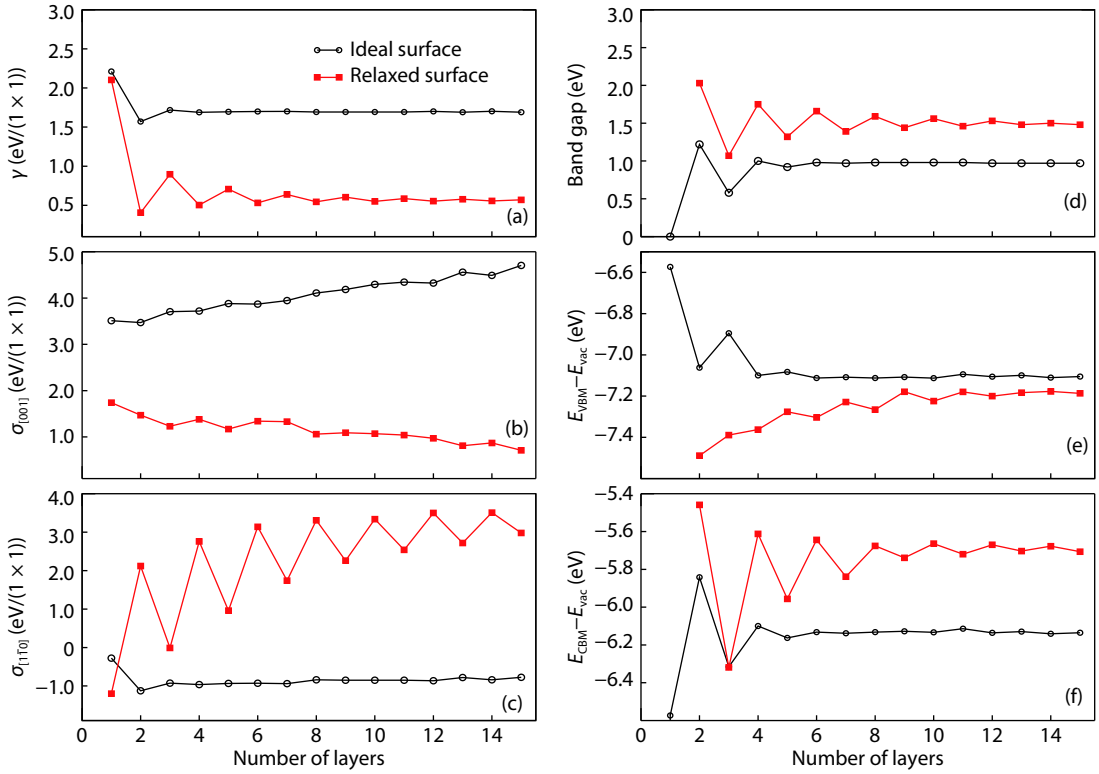

Fig. 1. (Color online) (a–c) Variations of surface energies and surface stresses, as well as (d–f) the electronic structure properties with the slab thickness. Black solid curves and red dashed curves are for the unrelaxed and relaxed surfaces, respectively. The valence band maximum (VBM,(e)) and the conduction band minimum (CBM,(f)) are referenced to the vacuum level. These figures are adapted from Ref. [14].

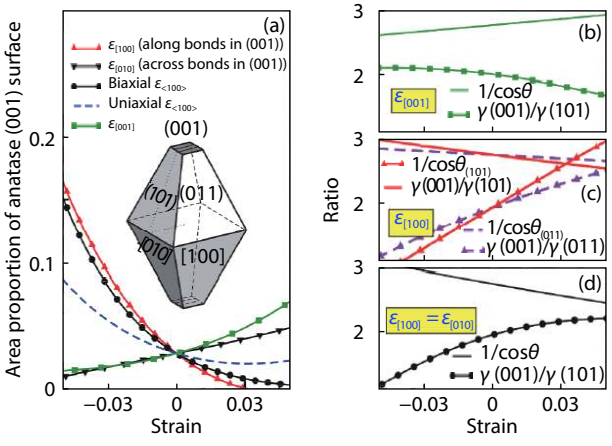

Fig. 2. (Color online) (a) The area percentage of anatase (001) facets with variation of the applied strain. The inset displays the equilibrium shape of the anatase crystallite. (b–d) The surface energy ratio $\gamma(001)/\gamma(101)$ and the ratio of $1/\cos\theta$ with the variation of the applied strain. The anatase (001) surface appears only when the surface energy ratio is smaller than $1/\cos\theta$. These figures are adapted from Ref. [13].

In addition, the in-plane OV formation energy remains almost constant at different depth, while the bridging and sub-bridging OVs formation energies appear a kind of odd-even oscillation behavior. With the position of OV going deeper, both of them tend to approach the formation energy of bulk OV[33, 34].

To get the influence of oxygen vacancies on the surface elasticity, we also calculated the vacancy-induced change of surface energy,

$$\Delta\gamma = \frac{E_r - E_s}{A_L} = \theta\frac{E_{OV} - \frac{1}{2}E_{O_2}}{A_{L0}}, \quad (4)$$

where θ is the density of vacancies and A_{L0} is the area per surface unit. The data of the vacancy-induced changes of surface stress $\Delta\sigma$ and surface elastic constants ΔS were thus obtained according to Eq. (1). In our calculations, a (2×2) supercell is used, and the corresponding defect density is $\theta = 1/4$. Lower defect density does not change the OV formation energies E_{OV} evidently. However, the values of $\Delta\gamma$, $\Delta\sigma$ and ΔS are proportional to OV density even when the density dependence of E_{OV} is ignorable, as indicated by Eq. (4).

The value of $\Delta\gamma$, $\Delta\sigma$ and ΔS induced by oxygen vacancies with $\theta = 1/4$ are listed in Table 3 and $\Delta\sigma$ and ΔS are shown in Fig. 4(b). It can be seen that the subbridging OV induces more tensile stress in $[1\bar{1}0]$ and less compressive stress in [001], as well as smaller elastic constants in both direction than that in the bridging one.

By substituting the data in Table 3 into Eq. (2), a phase diagram can be obtained for the most stable oxygen vacancy in the first trilayer[11]. As shown in Fig. 5, the sub-bridging OV and the in-plane OV are the most favorable surface OV under the compressive and tensile biaxial strain, respectively. In contrast, the bridging OV is most favorable when a tensile strain is applied along $[1\bar{1}0]$ and meanwhile a compressive strain is along [001]. Calculations on the formation of OV in bulk TiO_2 also suggest that the OV is more easily formed when it sits in the titanium-contained (110) plane under tensile strain along the $[1\bar{1}0]$ direction, consistent with the surface situation[12].

It is worthy to mention that we did not realize until re-

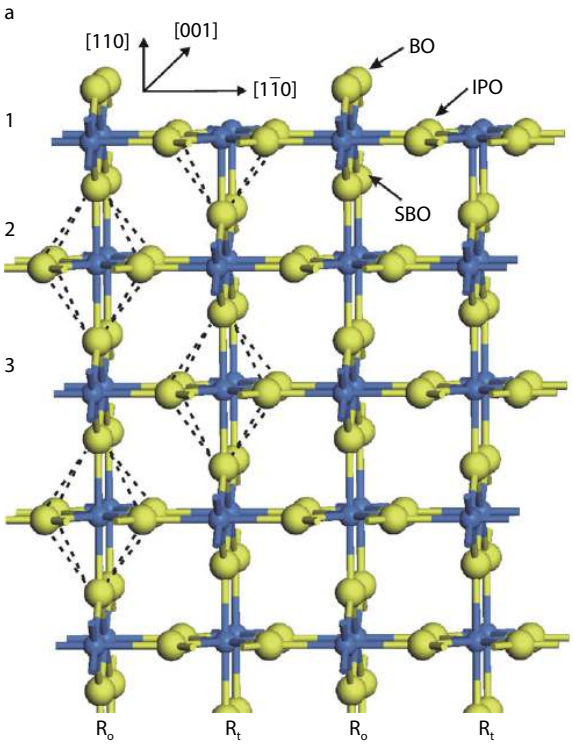

Fig. 3. (Color online) Schematic of the rutile TiO_2(110) surface. The bridging oxygen (BO), the subbridging oxygen (SBO) and the in-plane oxygen (IPO) atoms are indicated by the arrows. R_o and R_t denote the atomic rows in [110] direction, with surface terminated by the bridging oxygen atoms or the five-coordinated titanium atoms, respectively. This figure is adapted from Ref. [12].

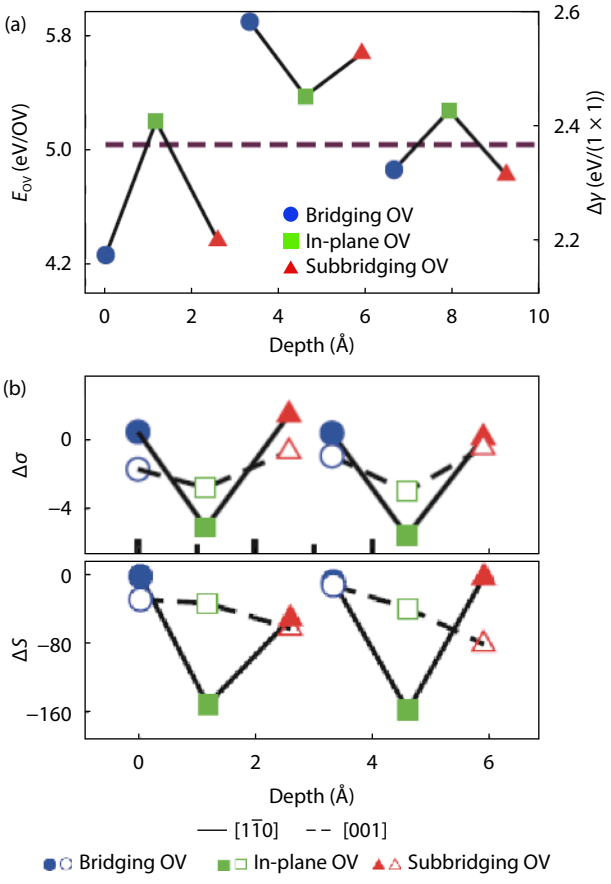

Fig. 4. (Color online) (a) The formation energy of OV and (b) the changes of the surface stresses and surface elastic constants induced by the OV as a function of the OV depth. The depth is defined as the distance below the unrelaxed 1-bridging O atoms. The dashed horizontal line in (a) denotes the bulk vacancy formation energy. Solid or dashed curves in (b) are to guide the eyes. $\Delta\sigma$ and ΔS are in units of eV/(1 × 1). These figures are adapted from Ref. [10].

cently that the incipient ferroelectricity of TiO_2 is also quite important for its surface properties. Under tensile strain, it tends to be more stable in the ferroelectric polarization state with lower symmetry[35–37]. However, we calculated the surface elasticity of OVs without intentionally reducing the symmetry. Therefore only if an OV could automatically break the symmetry, the tensile strain may drive the system to a polarization state[15]. We recently found that this occurs only when introducing an in-plane OV, whereas in the other cases the polarization state cannot be spontaneously reached although it is thermodynamically more stable under tensile strain. Therefore in more accurate calculations of the surface elasticity, one should take the polarization state into account.

5. Diffusion kinetics of oxygen vacancies

The distribution of defects can also be influenced by the diffusion kinetics. We have extensively studied the diffusion properties of OVs in TiO_2 and the effects of strain on the kinetics[12]. We found that the barrier is very high for an OV to directly hop along [001] direction, therefore the global energy barrier for an OV to diffuse either along [001] or [110] is determined by the path from the base planes to the apex positions of the Ti-O octahedrons. As shown in Fig. 6, this barrier decreases with increasing density of OV in the [001] direction. It indicates that the interaction between neighboring OVs facilitates the mobility of OVs in the bulk of TiO_2.

When a strain is applied along [001] direction or biaxially along [100] and [010], it would not break the symmetry. In this case, we found that the diffusion barrier is reduced by tensile strain and enhanced by compressive strain. If, however, the strain is just applied in [110] and [1$\bar{1}$0], it would increase the diffusion barrier of OVs whatever the strain is compressive or tensile. It also results in anisotropic diffusion behaviors along [110] and [1$\bar{1}$0]. Among the two otherwise equivalent directions, the bulk OV prefers to diffuse along the one under more compressive or less tensile strain, as indicated in Fig. 7.

Table 3. Changes of surface energy, surface stress and surface elasticity induced by different types of oxygen vacancies. The units are eV/(1 × 1). The subscripts 11 and 22 denote the directions along [1$\bar{1}$0] and [001] direction, respectively. This table is adapted from Refs. [10, 11].

Oxygen vacancy	$\Delta\gamma$	$\Delta\sigma_{11}$	$\Delta\sigma_{22}$	ΔS_{1111}	ΔS_{2222}	ΔS_{1122}
1-bridging	2.17	0.51	−1.66	−2.42	−29.36	−14.76
1-in-plane	2.40	−5.02	−2.73	−151.01	−34.03	−53.21
1-subbridging	2.21	1.50	−0.63	−51.67	−62.98	−44.09
2-bridging	2.58	0.43	−0.88	−8.38	−12.66	
2-in-plane	2.44	−5.51	−2.95	−157.96	−39.62	
2-subbridging	2.52	0.18	−0.41	−3.99	−81.19	

The diffusion barrier of OV on the surface is much lower than that of bulk OV. However, a highest diffusion barrier of OV occurs between the second trilayer and the third one, which hinders the OVs in bulk from diffusing to the

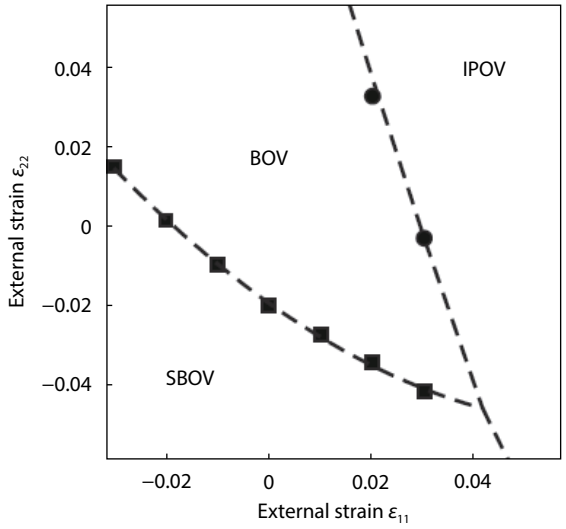

Fig. 5. Phase diagram of the type of the energetically most favorable OV as a function of the external strain ε_{11} and ε_{22}. The dashed curves are predicted according to the surface elasticity properties shown in Table 3. It indicates that BOV, IPOV, or SBOV can be energetically most favorable within different range of the external strain. This figure is adapted from Ref. [11].

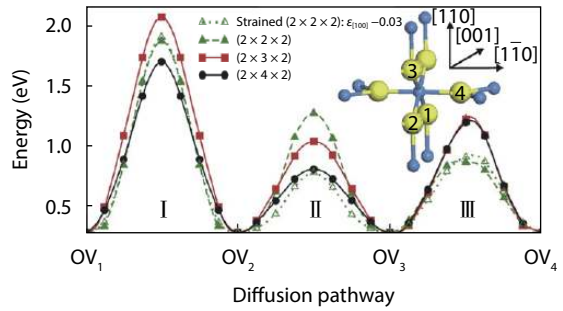

Fig. 6. (Color online) Energy profiles of OV pathways within the primitive cell of rutile TiO_2 using different size of supercell, namely (2 × 2 × 2), (2 × 3 × 2) and (2 × 4 × 2). The inset shows the schematic of a primitive cell. Large light spheres and small dark spheres denote the O and Ti atoms, respectively (the same below). The numbers label different oxygen atoms in order for reference of OVs. The notations I, II and III correspond to the paths from OV_1 to OV_2, from OV_2 to OV_3 and from OV_3 to OV_4, respectively. This figure is adapted from Ref. [12].

surface[12]. Externally applied tensile strain can reduce the energy barrier of the subsurface OV diffusion, and help to improve the diffusion of OVs from bulk to surface[12].

The diffusion of OVs within the (110) surface is also anisotropic. As shown in Fig. 8, the surface bridging OV diffuses more rapidly along [1$\bar{1}$0], mediated by the in-plane OV, with an energy barrier much smaller than in the bulk. The in-plane tensile strain lowers the diffusion barrier along both direction. With increasing tensile strain along [1$\bar{1}$0], the barrier along the [1$\bar{1}$0] decreases more significantly than along the [001] direction. Therefore the tensile strain along the [1$\bar{1}$0] direction further enhances the anisotropy in the surface diffusion[11].

6. Water adsorption and dissociation energy on s-TiO_2(110)

Since the hydroxyl ions and protons introduced by water dissociation play key roles in most relevant surface reactions, the adsorption and dissociation of water on TiO_2 surfaces have been extensively studied in the past years. We have found that the adsorption and dissociation of water on stoichiometric rutile (110) surface depend on both the coverage and the thin film thickness[14]. The adsorption energy was calculated as follows,

$$E_{M(D)} = (E_w - E_s)/2 - E_{H_2O}, \quad (5)$$

where E_w, E_s and E_{H_2O} stand for the total energy of water-adsorbed system, total energy of stoichiometric surface and the isolated water molecular respectively. The adsorption energies E_M and E_D correspond to the molecular and dissociation configurations, respectively. The dissociation energy is defined as $E_D - E_M$.

As shown in Fig. 9, both the adsorption and dissociation of water are energetically more favorable when the thin film has an odd O–Ti–O trilayers. Especially, when the adsorbed water has no neighboring one along the [001] direction, the dissociative water is more favorable on the TiO_2(110) surface of a thin film with three trilayer. This can be easily understood by referring to Fig. 1(a), since the slab containing an odd number of layers is less stable and thus more reactive than the one of even number of layers. With increasing thickness of the thin film or increasing coverage of the water, both the adsorption and the dissociation of water become less favorable.

The adsorption of water is more energetically favorable on thin films under tensile strain. Besides, the dissociation barrier of the water also decreases with increasing tensile strain[14]. Furthermore, the odd–even oscillation of the dissociation energy is enhanced by compressive strain, while reduced and even reversed by tensile strain. It means that under moderate tensile strain, the dissociation of water is more favorable on thin films containing even numbers of trilayers. This can be understood from the thickness-dependent surface stress. As shown in Figs. 1(b) and 1(c), the surface stress of the (110) thin film are positive. Therefore, tensile strain should increases their surface energy and thus their surface reactivity.

7. Adsorption and dissociation on reduced TiO_2(110): Effect of strain via polarization

As mentioned above, the rutile TiO_2 is a well-known incipient ferroelectric material. Previous theoretical studies suggested that the transition can occur under negative pressure or uniaxial strain. For the most stable TiO_2(110) surface, spontaneous in-plane polarization is predicted to occur under tensile strain. This strain-induced in-plane polarization is expected to play roles in the surface reactivity of the TiO_2(110) surface, which we have just explored[15].

By studying the adsorption of a series of molecules on the reduced TiO_2(110) surface under tensile strain, we found that the stabilities of the polarized structure relative to the non-polarized one are determined by the surface doping caused by the charge transfer between the adsorbates and the surface. The polarized structure favors the surface adsorption, and vice versa, if the adsorbate captures extra electrons of the reduced TiO_2 surface and introduces no additional holes. It is because the free carriers would screen the long-range Coulomb interactions and suppress the spontaneous po-

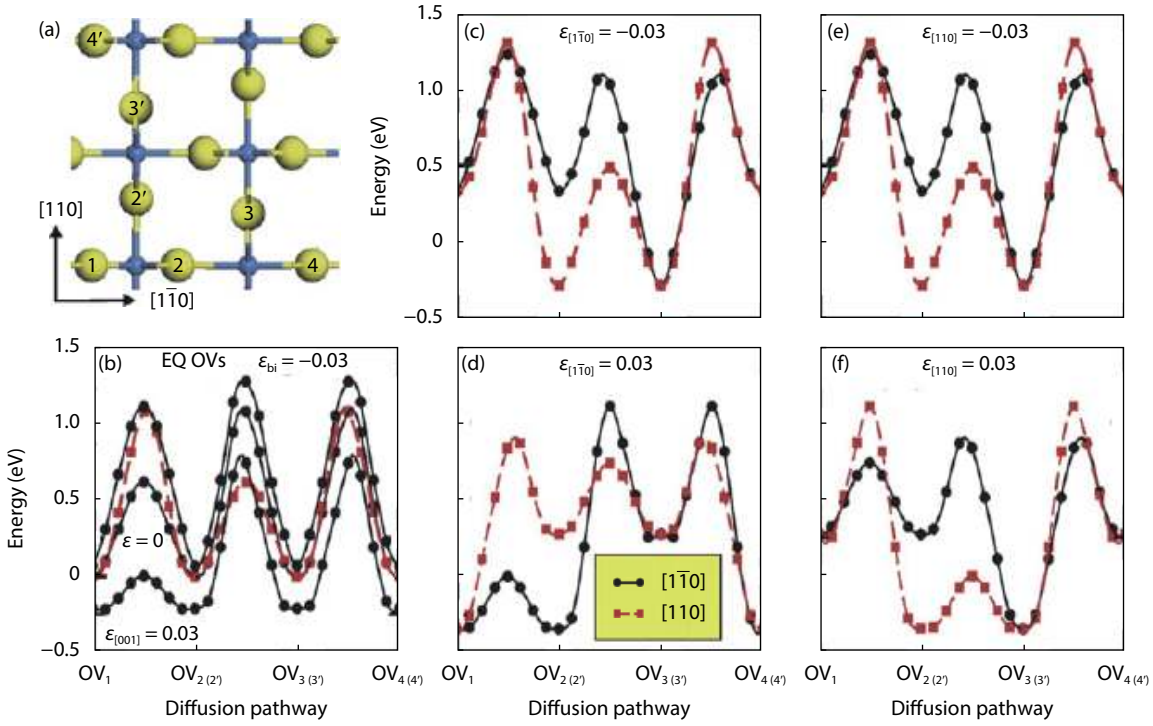

Fig. 7. (Color online) (a) Schematic of bulk OV diffusion along the [110] and [1$\bar{1}$0] directions in rutile TiO_2. The numbers label different oxygen atom sites for reference in (b–f). (b–f) The energy profiles of OV diffusion in rutile TiO_2, when (b) isotropic strain or anisotropic strain applied in directions along (c, d) [1$\bar{1}$0] and (e, f) [110]. These figures are adapted from Ref. [12].

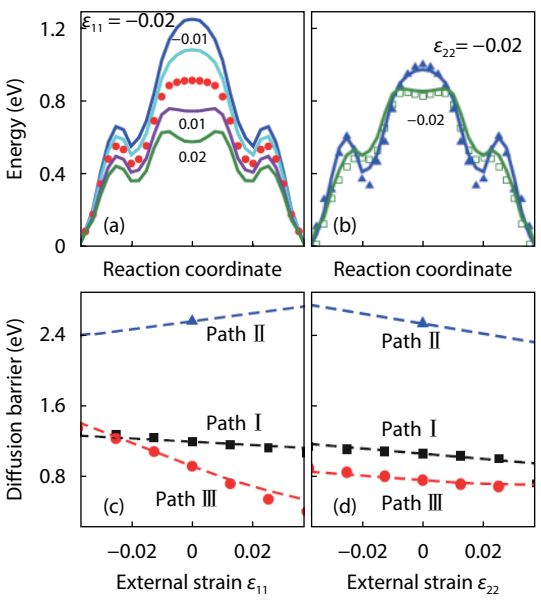

Fig. 8. (Color online) The strain-dependent diffusion barrier of the surface OV along [001] (Path I) and along [1$\bar{1}$0] (Path II, directive hopping between the bridging site; Path III, concerted mechanism mediated by the in-plane OV). Upper panels: The predicted energy profiles of the OV along Path III under external strain along (a) [1$\bar{1}$0] and (b) [001]. The solid lines are predicted according to the surface elasticity, and the symbols denote the calculated energy profiles using NEB method when $\varepsilon = 0$ (discrete circles), $\varepsilon_{22} = -0.02$ (discrete triangles) and $\varepsilon_{22} = 0.02$ (discrete squares) are also shown for comparison. Lower panels: the diffusion barriers of different pathways as a function of the external strain along the (c) [1$\bar{1}$0] direction and (d) [001] direction, with discrete points and dashed lines denoting the calculated and predicted values, respectively. These figures are adapted from Ref. [11].

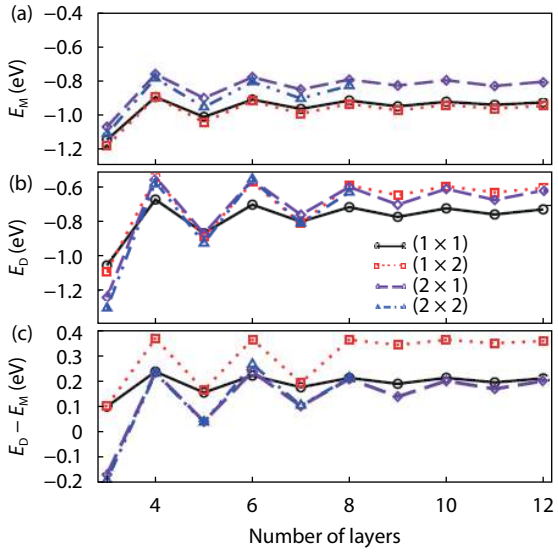

Fig. 9. (Color online) Adsorption energies per water molecule in (a) molecular state and (b) dissociative state on the surface with different supercell size and different thickness L_n. The differences between the adsorption energies of the dissociative state and the molecular state are shown in (c). The x and y direction of the surface is along [001] and [1$\bar{1}$0] direction, respectively. These figures are adapted from Ref. [14] by the permission of PCCP.

larization. The electrostatic interaction between the polar molecule and the in-plane polarization is of less importance relative to the effect of the surface doping.

The adsorbates we calculated were a series of chalcogen-containing molecules, including H_2O, H_2S, O_2 and CO_2, in molecular state and dissociative state. Since the molecular adsorption of H_2S is unstable against partial dissociation, we only con-

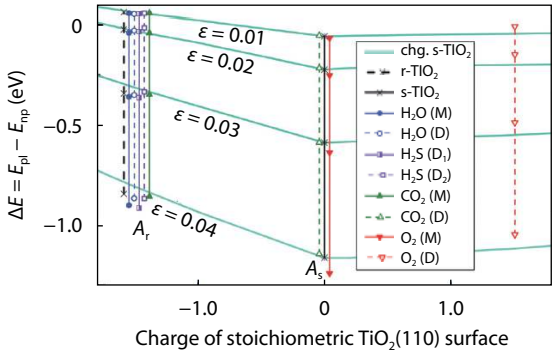

Fig. 10. (Color online) The change of the total energy of the s-TiO_2(110) surface induced by the in-plane polarization under strain along $[1\bar{1}0]$ as a function of the doped charge. Negative charge and positive charge correspond to electron doping and hole doping, respectively. This figure is adapted from Ref. [15] by the permission of PCCP.

sidered the adsorption of H_2S in a partial dissociative or complete dissociative state, denoted respectively as (D_1) and (D_2). The other molecules in molecular and dissociative states are hereafter denoted as (M) and (D), respectively.

We calculated the total energies of reduced TiO_2(110) after surface adsorption. The energies are denoted as E_a^{pl} and E_a^{np} for the stable strain-induced polarization state and the metastable non-polarization state, respectively. The difference $\Delta E_a = E_a^{pl} - E_a^{np}$ was calculated to demonstrate the polarization induced changes of the total energies of r-TiO_2 after surface adsorption. We found that the adsorbates can be clearly divided into two categories. For H_2O(M, D), H_2S(D_1, D_2) and CO_2(M), ΔE_a follows the variation of ΔE_r, *i.e.*, the energy difference of r-TiO_2(110). For CO_2(D) and O_2(M), ΔE_a equals approximately ΔE_s, *i.e.*, the energy difference of s-TiO_2(110). The two categories of adsorbates are hereafter denoted respectively as A_r and A_s. O_2(D) is intermediate between A_r and A_s since the total energy difference after adsorption of O_2(D) falls between ΔE_r and ΔE_s.

In order to understand the difference between the two different categories of adsorbates, the density of states (DOS) of r-TiO_2(110) with different adsorbates were compared. We found that the structures have similar ΔE_a if only they have similar Fermi levels, independent of the specific adsorbates. The bader analysis shows a consistent variation for the electronic doping of the surface by surface adsorption as the shift of the Fermi level does. In brief, the charge transfer between adsorbates A_r and r-TiO_2(110) is trivial, so that the surface remains doped with electrons by the oxygen vacancy. Instead, the adsorbates A_s heal the reduced surface and result into a neutral surface. Moreover, the adsorption of O_2(D) further dopes holes after healing the reduced surface.

In order to further verify the conclusion, we charged the polarized and non-polarized s-TiO_2(110) surface by simply adding and removing electrons, and then calculated the energy difference ΔE_s under the strain applied in $[1\bar{1}0]$ direction without further structural relaxation. As shown in Fig. 10, ΔE_s has a minimum when the surface is neutral, and increases with the amount of the charge (c) approximately linearly. We then plotted the polarization-induced energy difference of r-TiO_2(110), ΔE_r without adsorption and ΔE_a after adsorption, at a preset charge of s-TiO_2(110): c = −1.5 for ΔE_r or ΔE_a with adsorbates A_r, c = 0 for ΔE_a with adsorbates A_s, and c = +1.5 for ΔE_a after adsorption of O_2(D). We found that these energy differences match quite well with ΔE_s at the preset values of c. It confirms that the interaction between the in-plane polarization of TiO_2 surface and the adsorbate depends mainly on the surface doping by the adsorbate.

8. Summary

In this paper, we have reviewed our work within recent ten years on the strain engineering of TiO_2 surface properties. We found that when suitable external strain is applied in specific directions, the surface and bulk properties undergo a significant change, due to the difference in the elastic properties of different surface structures. We thus propose that the external strain is a good way to engineer the physical and chemical properties of TiO_2 and to further improve the catalytic reactivity. We hope our work will stimulate more experimental studies.

Acknowledgements

The numerical calculations were carried out at the High Performance Computing Center of Nanjing University. This work was supported by the National Natural Science Foundation of China (Grants No. 11974164).

References

[1] Asahi R, Morikawa T, Ohwaki T, et al. Visible-light photocatalysis in nitrogen-doped titanium oxides. Science, 2001, 293(5528), 269
[2] Campbell C T, Parker S C, Starr D E. The effect of size-dependent nanoparticle energetics on catalyst sintering. Science, 2002, 298(5594), 811
[3] Bikondoa O, Pang C L, Ithnin R, et al. Direct visualization of defect-mediated dissociation of water on TiO_2(110). Nat Mater, 2006, 5(3), 189
[4] Gratzel M. Photoelectrochemical cells. Nature, 2001, 414(6861), 338
[5] Lu G, Linsebigler A, Yates J T. Photooxidation of ch3cl on TiO_2(110) — a mechanism not involving H_2O. J Phys Chem, 1995, 99(19), 7626
[6] Pan X Y, Yang M Q, Fu X Z, et al. Defective TiO_2 with oxygen vacancies: Synthesis, properties and photocatalytic applications. Nanoscale, 2013, 5(9), 3601
[7] Yang B, Liu F, Lagally M G. Local strain-mediated chemical potential control of quantum dot self-organization in heteroepitaxy. Phys Rev Lett, 2004, 92(2), 4
[8] Lu G H, Cuma M, Liu F. First-principles study of strain stabilization of Ge(105) facet on Si(001). Phys Rev B, 2005, 72(12), 6
[9] Yin W J, Chen S Y, Yang J H, et al. Effective band gap narrowing of anatase TiO_2 by strain along a soft crystal direction. Appl Phys Lett, 2010, 96(22), 3
[10] Shu D J, Ge S T, Wang M, et al. Interplay between external strain and oxygen vacancies on a rutile TiO_2(110) surface. Phys Rev Lett, 2008, 101(11), 4
[11] Wang Z W, Shu D J, Wang M, et al. Diffusion of oxygen vacancies on a strained rutile TiO_2(110) surface. Phys Rev B, 2010, 82(16), 7
[12] Wang Z W, Shu D J, Wang M, et al. Strain effect on diffusion properties of oxygen vacancies in bulk and subsurface of rutile TiO_2. Surf Sci, 2012, 606(3/4), 186
[13] Jia L, Shu D J, Wang M. Tuning the area percentage of reactive surface of TiO_2 by strain engineering. Phys Rev Lett, 2012, 109(15), 5
[14] Yang L, Shu D J, Li S C, et al. Influence of strain on water adsorption and dissociation on rutile TiO_2(110) surface. Phys Chem Chem Phys, 2016, 18(22), 14833

[15] Wang Z W, Shu D J. Intrinsic interaction between in-plane ferroelectric polarization and surface adsorption. Phys Chem Chem Phys, 2019, 21(34), 18680
[16] Shojaee E, Mohammadizadeh M R. First-principles elastic and thermal properties of TiO_2: A phonon approach. J Phys Condens Matter, 2010, 22(1), 8
[17] Sato H, Ono K, Sasaki T, et al. First-principles study of two-dimensional titanium dioxides. J Phys Chem B, 2003, 107(36), 9824
[18] Isaak D G, Carnes J D, Anderson O L, et al. Elasticity of TiO_2 rutile to 1800 K. Phys Chem Miner, 1998, 26(1), 31
[19] Cammarata R C. Surface and interface stress effects in thin-films. Prog Surf Sci, 1994, 46(1), 1
[20] Vittadini A, Casarin M, Selloni A. Chemistry of and on TiO_2-anatase surfaces by dft calculations: a partial review. Theor Chem Acc, 2007, 117(5/6), 663
[21] Lazzeri M, Vittadini A, Selloni A. Structure and energetics of stoichiometric TiO_2 anatase surfaces. Phys Rev B, 2001, 63(15), 9
[22] Diebold U, Ruzycki N, Herman G S, et al. One step towards bridging the materials gap: surface studies of TiO_2 anatase. Catal Today, 2003, 85(2–4), 93
[23] Wendt S, Schaub R, Matthiesen J, et al. Oxygen vacancies on TiO_2(110) and their interaction with H_2O and O_2: A combined high-resolution STM and DFT study. Surf Sci, 2005, 598(1–3), 226
[24] Thompson T L, Yates J T. Surface science studies of the photoactivation of TiO_2 – new photochemical processes. Chem Rev, 2006, 106(10), 4428
[25] Yim C M, Pang C L, Thornton G. Oxygen vacancy origin of the surface band-gap state of TiO_2(110). Phys Rev Lett, 2010, 104(3), 4
[26] Diebold U, Lehman J, Mahmoud T, et al. Intrinsic defects on a TiO_2(110)(1x1) surface and their reaction with oxygen: A scanning tunneling microscopy study. Surf Sci, 1998, 411(1/2), 137
[27] Wahlstrom E, Lopez N, Schaub R, et al. Bonding of gold nanoclusters to oxygen vacancies on rutile TiO_2(110). Phys Rev Lett, 2003, 90(2), 4
[28] Schaub R, Wahlstrom E, Ronnau A, et al. Oxygen-mediated diffusion of oxygen vacancies on the TiO_2(110) surface. Science, 2003, 299(5605), 377
[29] Zhang Z R, Rousseau R, Gong J L, et al. Vacancy-assisted diffusion of alkoxy species on rutile TiO_2(110). Phys Rev Lett, 2008, 101(15), 4
[30] Kimmel G A, Petrik N G. Tetraoxygen on reduced TiO_2(110): Oxygen adsorption and reactions with bridging oxygen vacancies. Phys Rev Lett, 2008, 100(19), 4
[31] Klenov D O, Donner W, Foran B, et al. Impact of stress on oxygen vacancy ordering in epitaxial $(La_{0.5}Sr_{0.5})CoO_3$-partial derivative thin films. Appl Phys Lett, 2003, 82(20), 3427
[32] Kamisaka H, Yamashita K. The surface stress of the (110) and (100) surfaces of rutile 14 and the effect of water adsorbents. Surf Sci, 2007, 601(21), 4824
[33] Hameeuw K, Cantele G, Ninno D, et al. Influence of surface and subsurface defects on the behavior of the rutile TiO_2(110) surface. Phys Status Solidi A, 2006, 203(9), 2219
[34] Bredow T, Giordano L, Cinquini F, et al. Electronic properties of rutile TiO_2 ultrathin films: Odd-even oscillations with the number of layers. Phys Rev B, 2004, 70(3), 6
[35] Lee C, Ghosez P, Gonze X. Lattice-dynamics and dielectric-properties of incipient ferroelectric TiO_2 rutile. Phys Rev B, 1994, 50(18), 13379
[36] Parker R A. Static dielectric constant of rutile (TiO_2), 1.6–1060 °K. Phys Rev, 1961, 124(6), 1719
[37] Trayler J G, Smith H G, Nicklow R M, et al. Lattice dynamics of rutile. Phys Rev B, 1971, 3(10), 3457